Forecasting a class of bifurcations: Theory and experiment

Joosup Lim* and Bogdan I. Epureanu†

Department of Mechanical Engineering, University of Michigan, 2350 Hayward Street, Ann Arbor, Michigan 48109, USA

(Received 15 July 2010; revised manuscript received 25 October 2010; published 3 January 2011)

Forecasting bifurcations before they occur is a significant challenge and an important need in several fields. Existing approaches detect bifurcations before they occur by exploiting the critical slowing down phenomenon. However, the perturbations used in those approaches are limited to being very small and this represents a significant drawback. Large levels of perturbation have not been used mainly because of a lack of an adequate formulation that is robust to experimental noise. This paper provides such a formulation, and discusses how this approach to forecasting bifurcations is more accurate, especially when the dynamics are far from the bifurcation. Both numerical and experimental results are presented to demonstrate the technique and highlight its advantages over other prediction methods.

DOI: 10.1103/PhysRevE.83.016203 PACS number(s): 05.45.−a

I. INTRODUCTION

Forecasting bifurcations (i.e., predicting bifurcations before they occur) is a significant challenge, especially when an accurate model of the system of interest is not available. In this work, we focus on a certain class of bifurcations. Specifically, jump phenomena (via subcritical and/or saddle-node bifurcations) are important in many applications because they correspond to sudden and dramatic changes in the system dynamics. These types of nonlinear phenomena have been observed and discussed in a variety of systems (e.g., physical systems governed by equations of motion such as the Schrödinger equation [1] or the Swift-Hohenberg equation [2]), climate systems [3], ecological systems [4,5], biomedical systems (exhibiting behaviors such as asthma [6] or epileptic seizures [7,8]), neuron systems (exhibiting pulse propagation [9]), and global finance systems [10].

Several system characteristics have been explored for forecasting bifurcations of interest (e.g., noise-induced spectrum [11], virtual Hopf phenomenon [12], skewness of probability distributions [13], or flickering in bistable regions before bifurcations [14,15]). In particular, the critical slowing down phenomenon [16] has been employed as the underlying physical basis of various existing approaches for forecasting the occurrence of bifurcations [17]. Consider an attractor of the dynamics of a system (e.g., a stable fixed point, a stable limit cycle, or a chaotic attractor). When a small perturbation is applied to the system, the dynamics converge toward the attractor at some (recovery) rate. The critical slowing down means that this recovery rate approaches zero as a parameter of the system varies and the size of the basin of attraction shrinks to nil [18]. As a consequence, in the prebifurcation regime, the recovery rates (from small perturbations) decrease as the system approaches the bifurcation. These effects can be observed quite far from the bifurcation [17]. Hence, quantifying the effects of the critical slowing down is one method which can be used as an indicator of nearby bifurcations.

Nearby bifurcations have been predicted in various complex systems by monitoring the recovery rates of the system from *small* perturbations. Methods used have included monitoring changes in the autocorrelation [19] or the variance [20] of the system response to small perturbations (which are consequences of the critical slowing down [17]). These techniques for forecasting bifurcations have been studied for various systems, such as ecosystems [20–22], climate dynamics [23], cell signaling [24], and ocean dynamics [19]. Such studies are still far from being able to predict or forecast the most complicated bifurcations when an accurate model of the system is not available. Furthermore, in current techniques there are often two implicit assumptions that the dynamics of the system takes place on a very low dimensional manifold, and that the bifurcations are codimension one. Even more importantly, when a physical system is available for testing, the level of perturbations which can be applied to the system have to be very small. That is because the formulations based on observations of critical slowing down have been derived in close proximity to the attractor (by linearization after eliminating higher order terms).

In this paper, an alternate approach to characterizing the recovery rates of dynamical systems is proposed. Specifically, the rate of change of the amplitude of the dynamics (including certain higher order terms) is quantified. This new characterization shows that critical slowing down can also be observed when using much larger levels of perturbation. By tracking the change of the recovery rate from large perturbations, it is possible to predict both stable and unstable branches in a bifurcation diagram. Of course, when an accurate numerical model is available, bifurcation branches can be computed using several computational bifurcation tools (e.g., AUTO [25], MATCONT [26], DDE-BIFTOOL [27], and PDDE-CONT [28]). Only a few recent studies consider detecting unstable periodic orbits in the bifurcation diagram experimentally [29–31]. These approaches use controllers to stabilize unstable orbits and track them while a parameter of the system is varied. Such approaches are useful in detecting many types of bifurcations. However, controller-based approaches have many requirements. In contrast, the proposed approach does not require a controller and does not need the parameter to vary (or to enter the postbifurcation region). Instead, this

*jooslim@umich.edu
†epureanu@umich.edu

approach predicts the bifurcation and the unstable branches simply by tracking the recovery rate of the system dynamics. These advantages come at the price of limiting the class of bifurcations which can be tracked. Specifically, only Hopf and saddle-node bifurcations can be handled. Nonetheless, the characterized recovery rates can be used to predict both the occurrence and the type of bifurcations (i.e., supercritical or subcritical) before they occur.

Numerical simulations and experimental results are provided to demonstrate the use of our technique for forecasting bifurcations. Limit cycle oscillations of a simple mechanical system are used in the experiments. To simulate bifurcations of limit cycle oscillations, properly designed nonlinear feedback excitations are applied so that the desired types of bifurcations take place in an otherwise linear system. Nonlinear feedback excitations have been employed in structural health monitoring [32,33] and sensing [34] as an active interrogation approach. However, the feedback control, in this paper, is only used as a tool to simulate a desired nonlinear dynamics. The proposed approach does not require any type of control to be applied. As the time scale of the system used herein is very short (compared to several systems used in current studies [17]), our experimental setup provides large amounts of data in a short time. Moreover, the results obtained using the proposed approach suggest that predictions of bifurcations by critical slowing down can be sufficiently accurate for applications to engineered systems which generally require high precision (such as sensing). Many of the engineered systems experience the class of bifurcations of interest here (subcritical or supercritical Hopf bifurcations and/or saddle-node bifurcations), for example, relief valves [35], shape memory oscillators [36], aeroelastic systems [37], machine tools [38], and automotive components such as torque converter clutches [39].

II. THEORY

This section presents a method to forecast bifurcations by using time series collected *only* in the prebifurcation regime. The method is based on observation of how the system recovers to its equilibrium state from perturbations. Such a recovery of the oscillation amplitude to equilibrium is shown in Fig. 1. Discussion focuses on forecasting codimension-one supercritical or subcritical Hopf bifurcations and saddle-node bifurcations.

Consider a nonlinear system with the perturbed dynamics characterized by an amplitude r, and a fixed point or periodic dynamics characterized by an amplitude $\tilde{r}$. Consider also that a perturbation with a certain level r_0 is applied initially to the system. When the system has a stable behavior, it converges from the initial perturbation r_0 back onto the (stable) fixed point or the (stable) limit cycle of amplitude $\tilde{r}$ as shown in Fig. 1. When the system has an unstable fixed point or an unstable limit cycle, the amplitude r diverges away from $\tilde{r}$. The time rate of change of the amplitude in either of these cases is considered to be of the form,

$$\dot{r} = r[\alpha(\mu - \mu_c) - p(r)], \tag{1}$$

where α is a fixed parameter of the system, μ is a controlled and monitored parameter of the system, μ_c is the critical value of the parameter μ where a bifurcation occurs, and $p(r)$ is a polynomial function of r with $p(0) = 0$. Note that $p(r)$ is assumed to be independent of the control parameter μ. This is an important assumption which delineates the range of application of the proposed method. Here $\alpha > 0$, and the prebifurcation regime corresponds to $\mu < \mu_c$. In the prebifurcation regime, the dynamics of the system has a fixed point at $r = 0$. In the postbifurcation regime, the dynamics has one fixed point at $r = 0$ and another at $\tilde{r}$, where $\tilde{r}$ is given by $p(\tilde{r}) = \alpha(\mu - \mu_c)$. Furthermore, note that, in general, α is not known unless an accurate model for the system is available. Herein, we consider α an unknown that has to be identified or detected.

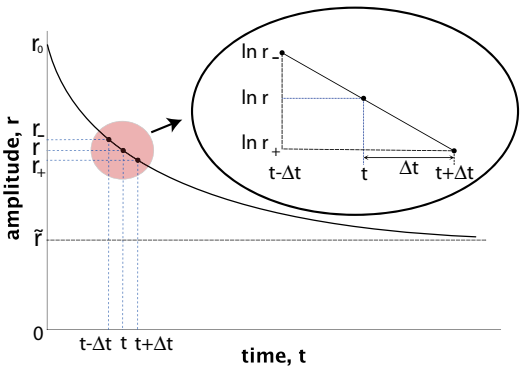

FIG. 1. (Color online) The rate function λ can be measured at each level of perturbation by measuring r_-, r, and r_+ at times $t - \Delta t$, t, and $t + \Delta t$. Note that perturbations do not have to be small. Only Δt needs to be small.

The rate of change of the phase θ of the system is not considered because we do not focus on infinite period bifurcations or other similar bifurcations. The phase of the system can be defined for any system exhibiting a limit cycle oscillation of period T to reveal the fact that the dynamics is periodic. Hence, θ varies by 2π when time varies by T. Only a generic phase definition is needed because the proposed approach uses only the amplitude of the oscillations as input data (and the system response is assumed to be periodic). Hence, θ and $\dot{\theta}$ do not significantly influence the analytic formulation.

The rate of amplitude variation at time t is defined as

$$\lambda(\mu,r) = \frac{d \ln r}{dt}. \tag{2}$$

Using Eq. (1) one obtains

$$\lambda(\mu,r) = \frac{1}{r}\dot{r} = \alpha(\mu - \mu_c) - p(r). \tag{3}$$

The rate of amplitude variation λ in Eq. (3) is a function of μ (the controlled or measured parameter) and r (the amplitude at time t), and is composed of two terms. The first term $\alpha(\mu - \mu_c)$ is the distance from the current parameter value μ to the critical value μ_c scaled by the fixed coefficient α. The second term $p(r)$ is a polynomial which characterizes the type of bifurcation.

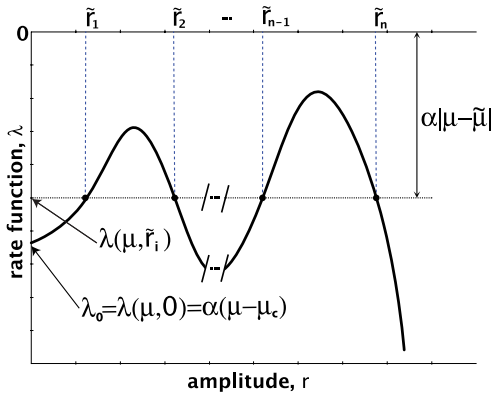

(a)

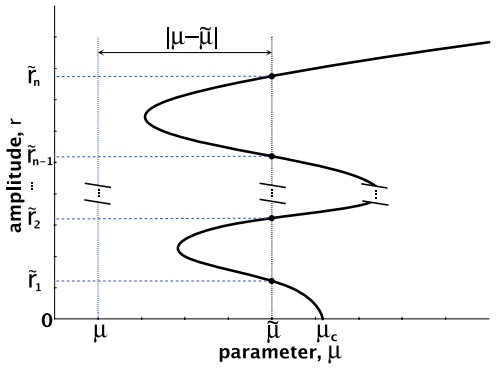

(b)

FIG. 2. (Color online) (a) Sketch of the dependence of λ on r for a fixed μ. (b) Bifurcation diagram for the parameter μ. Once λ is obtained for a certain μ, the shape of the actual bifurcation can be predicted without exploring the postbifurcation regime. For each i, $\lambda(\mu,\tilde{r}_i) = \alpha(\mu - \tilde{\mu})$ and the actual distance between μ and $\tilde{\mu}$ can be estimated (for a known α). Note that α can be easily obtained by measuring (as few as only) two values of λ for two distinct values of μ.

Consider that measurements are collected at times $t - \Delta t$, t, and $t + \Delta t$ to obtain three amplitudes r_-, r, and r_+ as shown in Fig. 1. To determine λ, one can employ the following approximation:

$$\lambda(\mu,r) = \frac{d \ln r}{dt} \cong \frac{\ln r_+ - \ln r_-}{2\Delta t}, \tag{4}$$

which holds for small Δt. Note that the measured perturbations r_-, r, and r_+ do not have to be infinitesimal as long as Δt is small.

Generally, λ can be exploited in either the r-λ space or the μ-λ space. First, consider the dynamics of the system for a fixed parameter μ and a varying perturbation level r. As shown in Fig. 2(a), the dependence of λ on r is a polynomial given by

$$\lambda(\mu,r) = \lambda_0 - p(r), \tag{5}$$

where $\lambda_0 = \alpha(\mu - \mu_c)$ represents the rate of amplitude variation when r tends to zero, $\lambda(\mu,r = 0)$. Different polynomials $p(r)$ correspond to distinct types of bifurcations. Therefore, the shape of $\lambda(\mu,r)$ in the r-λ space can be used to determine the type of bifurcation which takes place at $\mu = \mu_c$. Note that the bifurcation is forecasted, that is, it is identified *before* it takes place (using only μ values which are less than μ_c). This ability to forecast is not found in other existing techniques [25–31].

In general, for a given parameter value $\mu = \tilde{\mu}$, a system may have several coexisting fixed points or limit cycles. Consider the amplitude $\tilde{r}_i$ of one of those stable or unstable fixed points or limit cycles. As shown in Fig. 2(b), all points $(\tilde{\mu},\tilde{r}_i)$ on the bifurcation curve satisfy the equation of motion and correspond to fixed points for r. Hence,

$$\dot{r}(\tilde{\mu},\tilde{r}_i) = \tilde{r}_i\,[\alpha(\tilde{\mu} - \mu_c) - p(\tilde{r}_i)] = 0. \tag{6}$$

Now, recall the dependence of λ on r expressed in Eq. (3) [and presented in Fig. 2(a)]. For all $\tilde{r}_i$, the value of $\lambda(\mu,\tilde{r}_i)$ is the same, as we show here:

$$\begin{aligned}\lambda(\mu,\tilde{r}_i) &= \alpha(\mu - \mu_c) - p(\tilde{r}_i) \\ &= \alpha(\mu - \tilde{\mu} + \tilde{\mu} - \mu_c) - p(\tilde{r}_i).\end{aligned} \tag{7}$$

Using Eq. (6), one obtains

$$\begin{aligned}\lambda(\mu,\tilde{r}_i) &= \alpha(\mu - \tilde{\mu}) + \cancel{\alpha(\tilde{\mu} - \mu_c) - p(\tilde{r}_i)}^{\,0} \\ &= \alpha(\mu - \tilde{\mu}).\end{aligned} \tag{8}$$

Equation (8) reveals the fact that the value of λ at $\tilde{r}_i$ represents the distance (scaled by α) from the current μ to $\tilde{\mu}$. Note that for each i, $\lambda(\mu,\tilde{r}_i)$ is a line in the μ-λ space, which has the slope of α and crosses the μ axis ($\lambda = 0$) at $\tilde{\mu}$. An example of such a line [defined by Eq. (8)] is shown in Fig. 4. One can measure $\lambda(\mu,\tilde{r}_i)$ for as few as two distinct values of μ to obtain this line. This requirement is distinct from classical approaches where μ has to have many values which span both the prebifurcation and the postbifurcation regimes. Next, the fixed coefficient α can be estimated as it is the slope of the line [defined by Eq. (8)]. One can then measure λ (for a given value of $\tilde{r}$, and a given value of μ) and compute $\tilde{\mu}$ as

$$\tilde{\mu} = \mu - \frac{1}{\alpha}\lambda(\mu,\tilde{r}). \tag{9}$$

Finally, the bifurcation diagram can be predicted by the set of points $(\tilde{\mu}, \tilde{r})$.

Note that λ is derived without eliminating higher order terms. Hence, its definition can be used at any level of perturbation. Based on the values of λ at large amplitudes, one may predict the distance to μ_c from the current μ by estimating $\lambda_0 = \alpha(\mu - \mu_c)$ from Eq. (5). In most cases, it is a challenge to observe the system dynamics (and estimate λ) from very small perturbations because the measurements of actual dynamics can be obscured by noise. Therefore, the estimated value of λ_0 is more accurate if obtained using data collected for sufficiently large amplitudes.

The general algorithm for forecasting the bifurcation diagram using this approach is as follows:

(1) For a given value of the parameter $\mu = \mu_k$ (with $k = 1 \cdots M$, where M is chosen by the user), a perturbation is applied to the system, and amplitude values r_j (with $j = 1 \cdots N$, where N is chosen by the user) are collected at various time instances t_{jk}.

(2) Using Eq. (4), the rate of amplitude variation $\lambda_{jk} = \lambda(\mu_k,r_j)$ is computed at time t_{jk} for all $j = 1 \cdots N$.

(3) The slope α_j of the line $\lambda(\mu_k,r_j)$ versus μ_k is computed for each r_j ($j = 1 \cdots N$). Note that these N values of α_j can be

averaged over j to obtain an average value of α for improved noise rejection.

(4) A value of $\tilde{\mu}_{jk}$ is obtained for each μ_k $(k = 1 \cdots M)$ and each r_j $(j = 1 \cdots N)$ using Eq. (9) (where $\tilde{r}$ has a value $\tilde{r}_j$ of r_j) and the slope α obtained at step 4. Note that these M values of $\tilde{\mu}_{jk}$ can be averaged over k to obtain an average value for $\tilde{\mu}_j$ for improved noise rejection.

The bifurcation diagram is finally obtained as the plot of $\tilde{r}_j$ versus $\tilde{\mu}_j$ for $j = 1 \cdots N$ (where $\tilde{r}_j = r_j$).

III. RESULTS

In this section we demonstrate our approach by applying it first to a numerical model and then to an experimental system.

A. Numerical results

Forward (supercritical) and backward (subcritical) Hopf bifurcations are considered. The governing equations of motion for systems with such bifurcations are of the form shown in Eq. (1). They are characterized by two different types of polynomials $p(r)$ as follows:

$$p_f(r) = \beta r^2, \tag{10}$$

$$p_b(r) = -\beta r^2 + \gamma r^4. \tag{11}$$

The values of $\beta = 1$ and $\gamma = 1$ are used to obtain numerical data. The values of μ_c and α from Eq. (1) are considered to be $\mu_c = 0$ and $\alpha = 1$. The results obtained for λ, and the predictions made for both bifurcations are presented in Figs. 3 and 5.

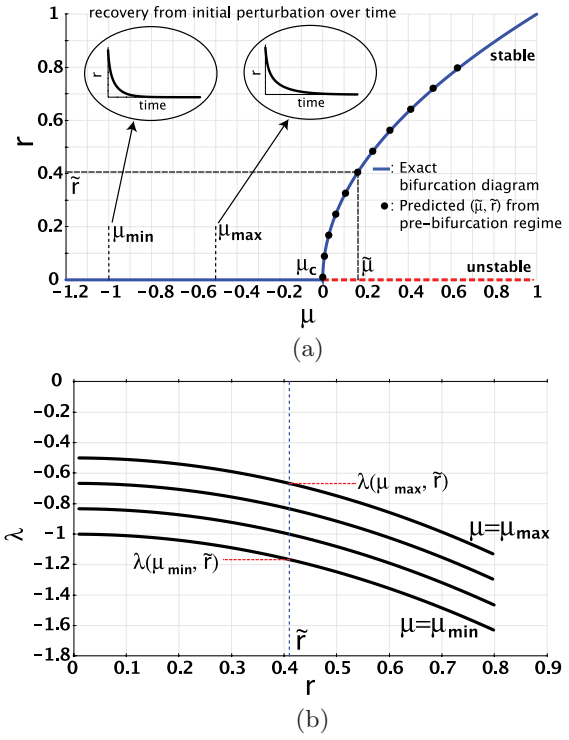

FIG. 3. (Color online) (a) Exact and predicted supercritical Hopf bifurcation. (b) λ versus r for a supercritical Hopf bifurcation. Predictions based on λ are demonstrated using a numerical model for a supercritical Hopf bifurcation.

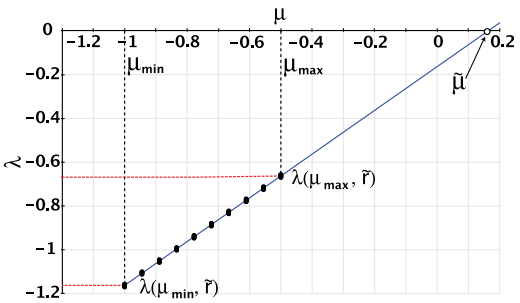

FIG. 4. (Color online) Each predicted point for $\tilde{r}$ in Fig. 3(a) is estimated by line fitting the measurements of $\lambda(\mu,\tilde{r})$ for various μ. The slope of the line fitting all measurements (for a given $\tilde{r}$) is α.

For a supercritical Hopf bifurcation, values for λ were obtained in a range of μ from $\mu_{\min} = -1$ to $\mu_{\max} = -0.5$, with a given initial perturbation amplitude $r_0 = 0.8$. The curve shown in Fig. 3(a) is the exact bifurcation diagram obtained by analytically solving $\dot{r} = 0$ for r at every μ between -1.2 and 1. The points $(\tilde{\mu}, \tilde{r})$ in Fig. 3(a) are predictions obtained by the proposed approach using multiple curves of λ collected for distinct values of μ between $\mu_{\min}$ and $\mu_{\max}$. Specifically, the values of λ for a certain amplitude $\tilde{r}$ on the dotted line shown in Fig. 3(b) are projected onto the μ-λ space as shown in Fig. 4. As discussed in Sec. II, this line has the slope of α and crosses the μ axis ($\lambda = 0$) at $\tilde{\mu}$. All predicted points shown in Fig. 3(a) are obtained by the same approach under the assumption that α is unknown (and must be measured). Note that, once α is identified, measurements of λ for a single μ value are sufficient to obtain a prediction for the entire bifurcation diagram in Fig. 3(a).

For a subcritical Hopf bifurcation, the range considered for μ was from $\mu_{\min} = -2$ to $\mu_{\max} = -1$, and the initial perturbation amplitude was $r_0 = 1$. The results shown in Fig. 5 were obtained by exactly the same procedure as for the supercritical Hopf bifurcation (Fig. 3). However, the curves obtained are distinct because the polynomial used to generate the (numerical) data is that given in Eq. (11) instead of Eq. (10). Additional important results are observed in the subcritical case. For example, the new approach can successfully predict the saddle-node bifurcation of cycles located at point S in Fig. 5(a). The predicted points approximate very well the exact location of the saddle-node bifurcation. In addition, the large amplitude of the emerging limit cycle at point S is captured accurately.

The predicted bifurcation diagrams obtained based on λ measured in the pre-bifurcation regime perfectly match the analytical diagrams for the numerical models of general Hopf bifurcations considered. The predicted information includes the locations of the bifurcation points, and the whole bifurcation diagram, including the unstable limit cycles. The curves of λ vs. r were obtained by tracking the time history of the system during its recovery from the initial perturbations.

Several time history plots shown as inserts in Figs. 3(a) and 5(a) demonstrate that it is not easy to discern specific bifurcation characteristics without proper analysis. Our approach presents a clear characterization of the time histories

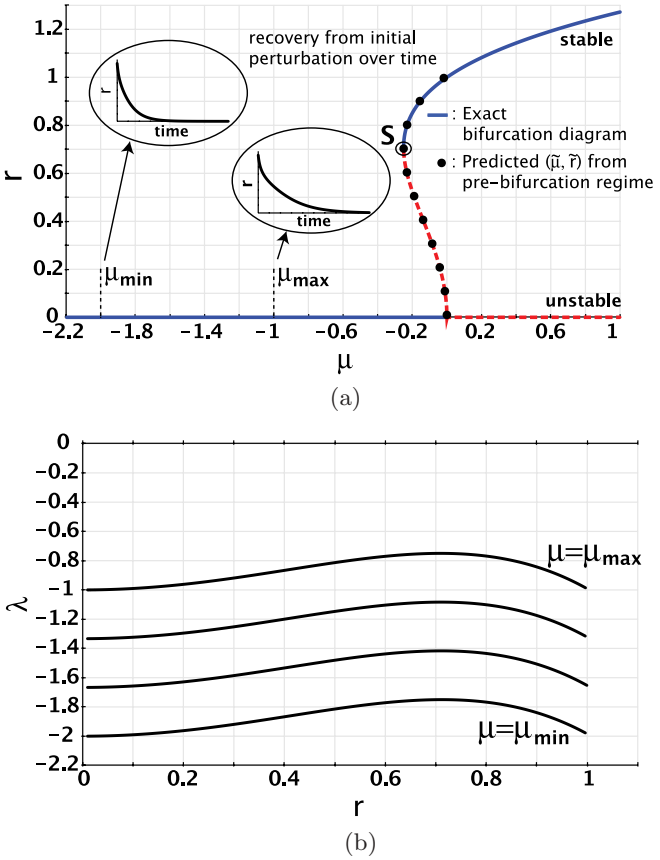

FIG. 5. (Color online) (a) Exact and predicted subcritical Hopf bifurcation. (b) λ versus r for a subcritical Hopf bifurcation. Predictions based on λ are demonstrated using a numerical model for a subcritical Hopf bifurcation.

both qualitatively (between different types of bifurcations), and quantitatively (between different values of μ for the same bifurcation). Our technique is experimentally demonstrated and verified in the next section for limit cycle bifurcations of a mechanical oscillatory system.

B. Experimental results

A clamped-free aluminum beam is used in the experiments. To induce supercritical or subcritical Hopf bifurcations in the system dynamics, nonlinear feedback excitations are applied to enhance the nonlinearity of the system [32]. A diagram of the experimental system is shown in Fig. 6. As shown in the figure, a piezo-sensor and a pair of piezo-actuators are attached to the aluminum beam. The sensor output signal is conditioned through a charge amplifier and is the input to a real-time processor. In the real-time processor, the sensor output data are stored while the data are also used to form a designed nonlinear feedback excitation, which is then amplified and sent to the piezo-actuators on the beam. Note that the feedback controller is not a requirement of the proposed approach to forecast bifurcations, but is used only for creating a system which exhibits the desired bifurcations. The proposed approach only uses the time-series data from the sensor. The controller actuation is used to provide an excitation which repeatedly induces large level perturbations to the system. That is done

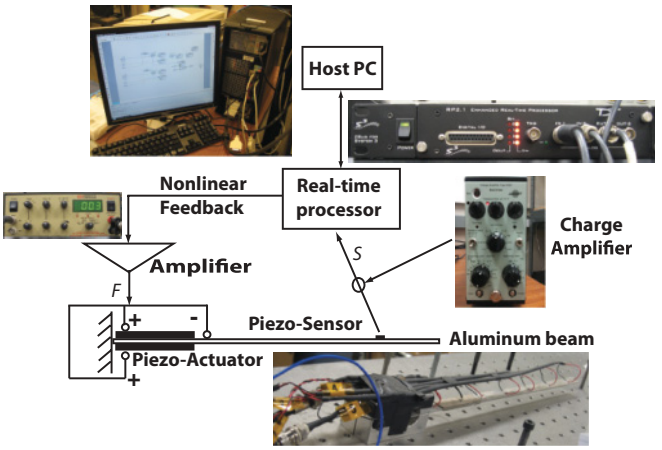

FIG. 6. (Color online) An aluminum beam is used for experimental tests. Nonlinear feedback is designed and applied to generate supercritical or subcritical Hopf bifurcations. Only one of the sensors on the beam is used in these experiments. From the piezo-sensor output signal s which is proportional to the amplitude of oscillation, nonlinear feedback F is formed and applied to the base of the beam (as a locally distributed bending) by a pair of piezo-actuators.

for the sake of experimental validation and is not needed when other external perturbations exist or can be easily applied. Also, note that the large level perturbations applied do not have to be identical.

To induce desired supercritical or subcritical Hopf bifurcations, nonlinear feedback is generated from the piezo-sensor output signal s which is proportional to the oscillation amplitude. The nonlinear feedback is applied to the beam (as a locally distributed bending) by a pair of piezo-actuators attached on both (upper and lower) sides of the beam. The nonlinear feedback F can be expressed as a function of the sensor output s as

$$F = \mu s + \beta s^3 + \gamma s^5, \tag{12}$$

where μ is the control parameter, and β and γ are the nonlinear feedback gains, which are fixed for each desired bifurcation. For creating a supercritical Hopf bifurcation, nonlinear gain parameters are fixed as $\beta = -0.01$ and $\gamma = 0$, with 20 dB of charge amplifier gain. For creating a subcritical Hopf bifurcation and a saddle-node bifurcation, nonlinear gain parameters are fixed as $\beta = 5$ and $\gamma = -0.05$, with 10 dB of charge amplifier gain. These parameters were chosen based on a few preliminary experimental tests.

One can also express the equation of motion for a finite element model of the beam with nonlinear feedback excitation as

$$\mathbf{M}\ddot{\mathbf{u}} + \mathbf{C}\dot{\mathbf{u}} + \mathbf{K}\mathbf{u} = \mathbf{G}s + \mathbf{N}_\beta \mathbf{p}_\beta(s) + \mathbf{N}_\gamma \mathbf{p}_\gamma(s), \tag{13}$$

where matrices $\mathbf{M}$, $\mathbf{C}$, and $\mathbf{K}$ are mass, damping, and stiffness matrices, $\mathbf{G}$ is a linear feedback gain matrix, $\mathbf{N}_\beta$ and $\mathbf{N}_\gamma$ are nonlinear feedback gain matrices, $\mathbf{u}$ is the vector of nodal displacements and rotations, and s is the sensor output. The vectors $\mathbf{p}_\beta(s)$ and $\mathbf{p}_\gamma(s)$ contain terms like s, s^2, s^3, s^4, and s^5. The details of such a model, however, are not discussed in this paper because the presented method does not require a numerical model. In fact, one of the advantages of the proposed

approach is precisely that it does not require an accurate model and can be applied experimentally.

Each experiment consists of two steps. The first step is to obtain the actual bifurcation diagram by the classic method of parameter sweeping. This step is performed so that the predictions obtained using our approach can be compared to the actual bifurcation diagram. To obtain the actual bifurcation diagram, the linear feedback gain (the controllable parameter μ) is changed from prebifurcation values to postbifurcation values in the parameter space. For subcritical bifurcations, a reverse sweep in the parameter is also applied (to capture the jump phenomenon at the saddle-node bifurcation of cycles). After ignoring transients, the amplitude of the limit cycle oscillations is obtained and plotted versus its corresponding parameter value to obtain a bifurcation diagram. The bifurcation diagram obtained by this classic method is shown in Fig. 8 in the form of dashed lines. Note that the lines in Figs. 8(b) and 8(c) which (at a first glance) may look like an imperfect bifurcation are an artifact of the plotting of the results. They are caused by the finite step size between each parameter value considered in the classical method. Lines (connecting actual measured points) are used instead of points for better visibility because the results of our approach are marked as circles (with error bars). Furthermore, the jump phenomena presented in Figs. 8(d)–8(f) are caused by subcritical Hopf bifurcation and saddle-node bifurcation. Note that the jump phenomena may also be observed for supercritical Hopf bifurcations as a delay effect for systems with slowly varying parameters [40]. However, in the experiment herein the applied nonlinear feedback is designed specifically to induce a subcritical Hopf bifurcation, and the parameters of the system are maintained constant long enough to reach steady state for each parameter value.

The second and critical step is to predict the bifurcation location and shape using only λ values obtained in the *prebifurcation* regime. To obtain the curve of λ for a fixed parameter μ, a perturbation is applied to the system. The perturbation is caused by a harmonic excitation (with a high frequency and a certain amplitude) which is applied to the system for a very short time, to provide a desired perturbation. After the perturbation, the dynamics of the system in its transient regime (as the system recovers from its perturbed state) are recorded. Specifically, the amplitude of the oscillation is measured during the transient phase. In this case, recovery is complete when the transients decay to zero. Note that the frequency of the short perturbations is chosen close to the resonant frequency of the system. Other types of perturbations can be applied, however, they may place more stringent restrictions on the data acquisition (sampling rate and resolution). Although interesting, the study of other perturbations is beyond the scope of this paper.

The resonant frequency of the system (close to the bifurcation) was measured experimentally and found to be approximately 6.1 kHz for both supercritical and subcritical Hopf bifurcations. The sampling rate of the data acquisition was approximately 200 kHz.

The measured dependence of λ on r for supercritical and subcritical Hopf bifurcations is shown in Fig. 7. For a given value of μ, a time series of 4000 individual r values was obtained as the system decayed to the equilibrium (zero) state.

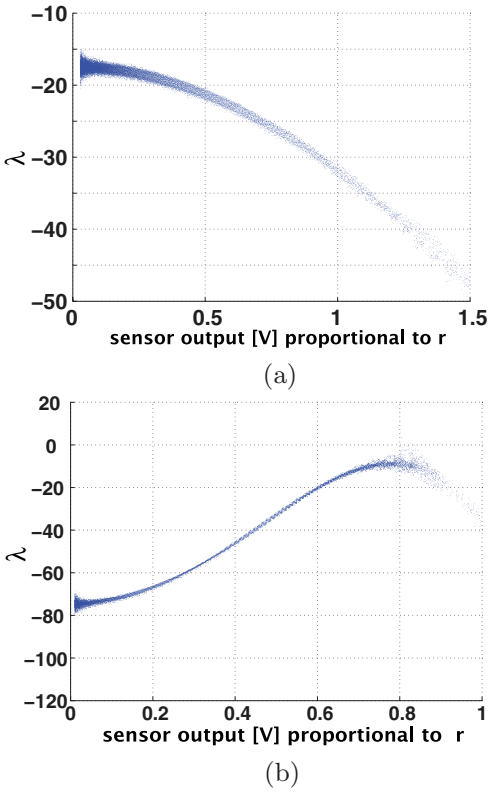

FIG. 7. (Color online) (a) λ for supercritical Hopf bifurcation ($\mu = 0.9$). (b) λ for subcritical Hopf bifurcation ($\mu = 2$). 4000 values of λ are obtained for distinct r values from a transient phase. The process is repeated 16 times for each μ value.

Then the values of λ were obtained using Eq. (4) for those r values. This process was repeated 16 times for each μ value. In obtaining λ values using Eq. (4), experimental noise can affect small values of r and lead to large errors in λ. Hence, r values below a preset minimum amplitude were eliminated. This minimum amplitude depends on the data acquisition system used. For the results herein, the value used was 50 mV. Note that our method is designed to provide estimates for the values of λ even when these values are small. This is accomplished by taking advantage of data obtained from larger perturbations, and by using the curves of λ in the r-λ plane. These results are demonstrated in Fig. 7, where the amplitude of the dynamics r is proportional to the output voltage of the sensor.

For the supercritical Hopf bifurcation, values of μ were chosen between $\mu_{\min} = 0.45$ and $\mu_{\max} = 0.95$. Similarly, for the subcritical bifurcation, μ values between $\mu_{\min} = 1$ and $\mu_{\max} = 2$ were used. Eleven distinct values of μ were selected for the experiments in each of these ranges. In the μ-λ space, line fitting was conducted to predict the location of each corresponding limit cycle amplitude (similar to what was done using numerical data to obtain the results in Fig. 4). Furthermore, the value of α was estimated based on the slopes of the lines in the μ-λ space. The value of α obtained for the supercritical Hopf bifurcation is $\alpha_f = 195.82$ (with a standard deviation of 1.56), and for the subcritical Hopf bifurcation is $\alpha_b = 66.81$ (with a standard deviation of 2.93). As shown in Fig. 8, the predictions using Eq. (9) match the actual bifurcation diagrams very well.

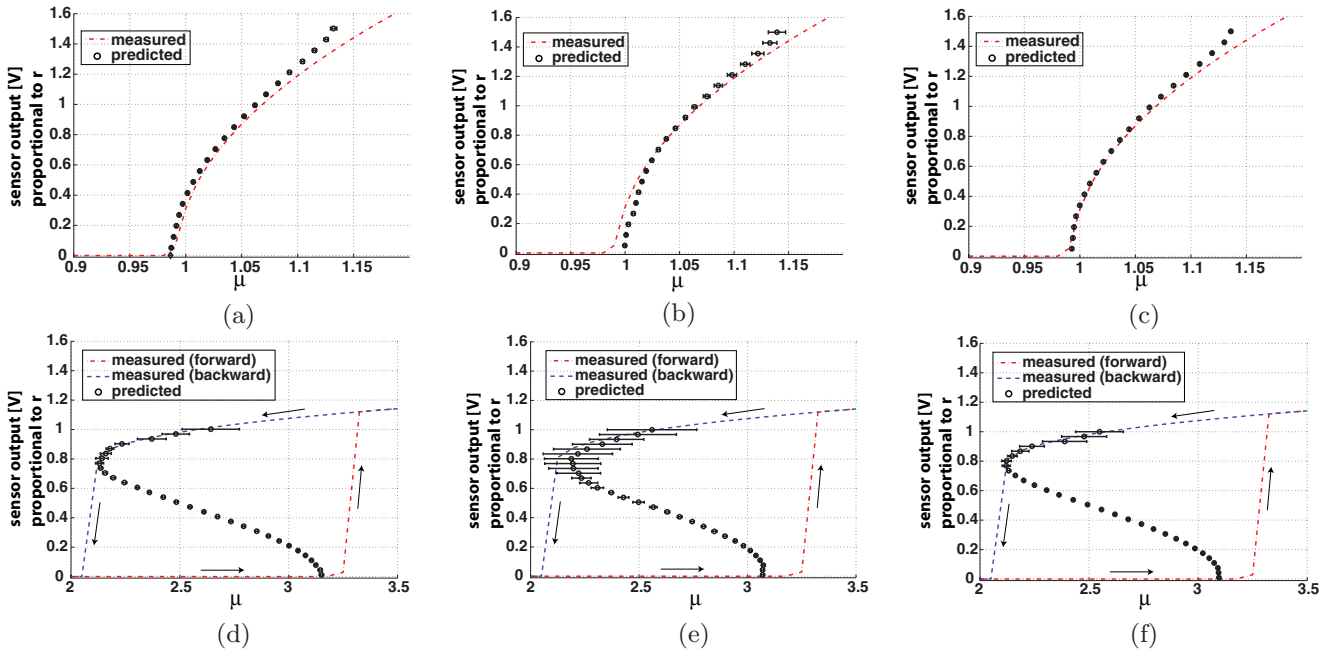

FIG. 8. (Color online) Predictions for the bifurcation diagram obtained based on λ are demonstrated for supercritical and subcritical Hopf bifurcations. (a) Based on multiple μ values; (b) $\mu = 0.45$; (c) $\mu = 0.95$; (d) based on multiple μ values; (e) $\mu = 1$; (f) $\mu = 2$. The upper plots (a)–(c) are for a supercritical Hopf bifurcation, and the lower plots (d)–(f) are for a subcritical Hopf bifurcation. The dashed lines represent the actual bifurcation diagram measured by applying actual parameter variations in the postbifurcation regime. Results show that predictions are more accurate when they are based on λ values obtained at multiple μ values. Furthermore, once α is calculated, predictions are most accurate when they are based on measurements at a value of μ close to the actual bifurcation (i.e., for μ close to μ_c). The horizontal bars represent standard deviation error bars computed for each predicted point on the bifurcation diagram.

Our results also show that a bifurcation can be predicted quite well even when measurements obtained at a single value of μ are used (once α is obtained). Note that in all measurements, μ is lower than the value where the system actually encounters the bifurcation (at μ_c).

Figures 8(b), 8(c), 8(e), and 8(f) present the predictions obtained using measurements at single values of μ. Figures 8(b) and 8(e) show results obtained using a value of μ which is $\mu_{\min}$, and is the farthest from the actual bifurcation (at μ_c). Figures 8(c) and 8(f) show results obtained using a value of μ which is $\mu_{\max}$, and is the closest to the actual bifurcation (at μ_c). As the parameter μ approaches its bifurcation value μ_c, the predictions based on λ are more accurate. Note, however, that the bifurcation is well predicted even when using measurements collected at $\mu_{\min}$. These measurements are quite far from the bifurcation (halfway between zero feedback and the actual bifurcation point). For the subcritical Hopf bifurcation [Figs. 8(d)–8(f)], one can observe a small difference between the actual and the predicted bifurcation points. However, these results are reliable, especially considering that the values of μ are chosen in a range well below μ_c (where the saddle node emerges).

IV. DISCUSSION AND CONCLUSIONS

A new method of characterizing the dynamics of a nonlinear system during its transient recovery to a stable limit cycle or a stable fixed point after perturbations (in the prebifurcation regime) was presented. The proposed approach is designed for forecasting bifurcations of fixed points or limit cycles. By keeping all higher order (nonlinear) information in the formulation, the perturbation levels do not have to be small. Allowing for large perturbations is important because it can be challenging to measure recovery from small perturbations due to a loss of accuracy caused by noise and/or a lack of resolution in measurement. In most cases, operating with larger perturbations is a good way to resolve such accuracy issues and obtain better predictions of the bifurcations without the need to explore the postbifurcation regime. Furthermore, the recovery rates obtained using large perturbations enable the prediction of locations in parameter space where the stable or unstable limit cycles lie as well as the amplitudes of those limit cycles.

Another important feature of the proposed method is its ability to accurately predict saddle-node bifurcations and unstable limit cycles for the case of subcritical Hopf bifurcations. There are several recent studies to experimentally follow unstable branches by means of feedback control. However, those studies differ fundamentally from the approach in this paper. The proposed method predicts the unstable branches without following them [i.e., in the prebifurcation regime (where the system always recovers to its equilibrium)]. From a practical standpoint, this is clearly the safest way to investigate a system. Furthermore, the use of feedback in this paper is only for the purpose of creating a well-known system which can be used for quantitative evaluation of the predictions our method provides. In contrast to other experimental techniques [29–31], the feedback is not needed (and not used) for forecasting the bifurcations or the unstable

branches. Due to its minimal requirements (i.e., time-series data), the proposed method has strong potential for application to other areas, such as biological systems or natural systems, where the implementation of feedback control for the purpose of forecasting bifurcations or measuring unstable branches may be difficult.

A clamped-free aluminum beam with a nonlinear feedback excitation was introduced for experimental verification of the proposed method. The oscillatory system with nonlinear feedback has several advantages for testing nonlinear techniques. First, desired types of bifurcations can be induced easily in the system because the nonlinearity of the system comes from the control feedback (which can be designed for each specific case of interest). Second, the predicted shape of the bifurcation can be obtained very quickly because (once α is known) a single time history of the recovery from a large perturbation contains all necessary information for the range of the corresponding amplitudes as well. This contrasts with classical techniques where the bifurcation parameter has to be varied and many steady-state curves have to be measured to obtain the bifurcation diagram. In addition, the results using the proposed approach are very accurate when compared with results of classical techniques.

In the experiments, the actuation (by the controller) was used to induce perturbations repeatedly. Multiple perturbations were used for two reasons: (1) to enhance the accuracy of the predictions, and (2) to develop a method to predict unstable branches, to be used precisely when the response of the system *is* available for multiple perturbations. Note that, when multiple perturbations are available, they do not have to be the same (e.g., they do not have to have a similar level). Some can be large and some small, or they can be large and of different levels. In fact, natural (small or large) perturbations can be used. The only requirement here is that the system recovers to its equilibrium state from these perturbations. For example, the proposed method (using time series) can be applied to a system which undergoes an impulse-type disturbance during operation (e.g., an aeroelastic system encountering a gust during flight) which causes (large or small) perturbations after which the system recovers to its regular (stable) operating conditions.

Of course, the proposed approach has restrictions on its applicability. First, the dynamics are assumed to be effectively one dimensional and periodic, and the bifurcation is assumed to be codimension one. Currently available techniques also consider limited types of dynamics and codimension-one bifurcations. These studies (and ours) are still far from being able to predict or forecast bifurcations for the most complex systems, especially when an accurate model of the system of interest is not available. Second, if the system does not experience large perturbations (either induced or natural), then one cannot fully take advantage of the proposed method. However, the proposed approach can still be used (in a limited sense) by monitoring small perturbations (either induced or natural) to locate the bifurcation point. Third, the perturbations are assumed to be of a magnitude which does not make the system switch between different attractors; that is, the assumption is that the system reverts to its initial equilibrium position (or to its initial periodic limit cycle oscillation) in time after the perturbation subsides. Fourth, the nonlinear terms are assumed to be independent of the control parameter. These restrictions are necessary when one needs to forecast the bifurcation (instead of detecting it by sweeping up and/or down a system parameter).

The proposed technique enables the use of larger perturbation levels which broadens its applicability as compared to existing techniques based on the critical slowing down. In addition to predicting where bifurcations occur, the proposed approach can be used to anticipate the type of the bifurcations (supercritical or subcritical) and predict their branches without exploring the postbifurcation regime. Due to the dramatic change in the dynamics at bifurcations, predicting subcritical and saddle-node bifurcations without placing the system in the postbifurcation regime provides great advantages in many applications.

ACKNOWLEDGMENTS

The authors acknowledge the National Science Foundation for the generous support of this work (Sensors and Sensing Systems Program directed by Dr. Shih-Chi Liu, Grant No. 0397327, and Dynamical Systems Program directed by Dr. Edwardo Misawa, Grant No. 0625011), and the two anonymous reviewers for their helpful comments, which greatly helped improve the manuscript.

[1] U. Bortolozzo, M. G. Clerc, and S. Residori, Phys. Rev. E **78**, 036214 (2008).
[2] A. Sacchetti, Phys. Rev. Lett. **103**, 194101 (2009).
[3] T. M. Lenton, H. Held, E. Kriegler, J. W. Hall, W. Lucht, S. Rahmstorf, and H. J. Schellnhuber, Proc. Nat. Acad. Sci. USA **105**, 1786 (2008).
[4] M. Scheffer, S. Carpenter, J. Foley, C. Folke, and B. Walker, Nature (London) **413**, 591 (2001).
[5] M. Parkes, Ecohealth **3**, 136 (2006).
[6] J. Venegas, T. Winkler, G. Musch, M. Melo, D. Layfield, N. Tgavalekos, A. Fischman, R. Callahan, G. Bellani, and R. Harris, Nature (London) **434**, 777 (2005).
[7] B. Litt *et al.*, Neuron **30**, 51 (2001).
[8] P. McSharry, L. Smith, and L. Tarassenko, Nature Medicine **9**, 241 (2003).
[9] D. Golomb and G. B. Ermentrout, Phys. Rev. Lett. **86**, 4179 (2001).
[10] R. M. May, S. A. Levin, and G. Sugihara, Nature (London) **451**, 893 (2008).
[11] C. Jeffries and K. Wiesenfeld, Phys. Rev. A **31**, 1077 (1985).
[12] K. Wiesenfeld, Phys. Rev. A **32**, 1744 (1985).
[13] V. Guttal and C. Jayaprakash, Ecol. Lett. **11**, 450 (2008).
[14] S. R. Carpenter, W. A. Brock, J. J. Cole, J. F. Kitchell, and M. L. Pace, Ecol. Lett. **11**, 128 (2008).
[15] N. Berglund and B. Gentz, Stochastics and Dynamics **2**, 327 (2001).

[16] S. H. Strogatz, *Nonlinear Dynamics and Chaos with Applications to Physics, Biology, Chemistry, and Engineering*, 1st ed. (Westview Press, Boulder, 2001).
[17] M. Scheffer, J. Bascompte, W. A. Brock, V. Brovkin, S. R. Carpenter, V. Dakos, H. Held, E. H. van Nes, M. Rietkerk, and G. Sugihara, Nature (London) **461**, 53 (2009).
[18] C. Wissel, Oecologia **65**, 101 (1984).
[19] T. Kleinen, H. Held, and G. Petschel-Held, Ocean Dynamics **53**, 53 (2003).
[20] S. Carpenter and W. Brock, Ecol. Lett. **9**, 308 (2006).
[21] R. A. Chisholm and E. Filotas, J. Theor. Biol. **257**, 142 (2009).
[22] E. H. van Nes and M. Scheffer, Am. Nat. **169**, 738 (2007).
[23] V. Dakos, M. Scheffer, E. H. van Nes, V. Brovkin, V. Petoukhov, and H. Held, Proc. Nat. Acad. Sci. USA **105**, 14308 (2008).
[24] C. P. Bagowski and J. E. Ferrell Jr., Curr. Biol. **11**, 1176 (2001).
[25] E. Doedel, A. Champneys, T. Fairgrieve, Y. Kuznetsov, B. Sandstede, and X. Wang, computer code AUTO97: Continuation and bifurcation software for ordinary differential equations, Concordia University, Montreal, Canada, 1998.
[26] A. Dhooge, W. Govaerts, Y. Kuznetsov, W. Mestrom, A. Riet, and B. Sautois, computer code MATCONT and CL_MATCONT: Continuation toolboxes in MATLAB, 2006.
[27] K. Engelborghs, T. Luzyanina, and D. Roose, ACM Trans. Math. Soft. **28**, 1 (2002).
[28] R. Szalai, computer code PDDE CONT: a continuation and bifurcation software for delay-differential equations, 2005.
[29] J. Sieber, A. Gonzalez-Buelga, S. A. Neild, D. J. Wagg, and B. Krauskopf, Phys. Rev. Lett. **100**, 244101 (2008).
[30] J. Sieber and B. Krauskopf, Nonlinear Dynamics **51**, 365 (2008).
[31] D. A. W. Barton and S. G. Burrow, ASME Conf. Proc. **2009**, 361 (2009).
[32] S. H. Yin and B. I. Epureanu, J. Fluids Struct. **21**, 543 (2005).
[33] K. D'Souza and B. I. Epureanu, Proc. R. Soc. London A **464**, 3129 (2008).
[34] K. D'Souza and B. I. Epureanu, J. Sound Vib. **329**, 2463 (2010).
[35] A. Maccari, Nonlinear Dynamics **22**, 225 (2000).
[36] V. Piccirillo, J. M. Balthazar, and B. R. Pontes, Nonlinear Dynamics **59**, 733 (2010).
[37] K. W. Chung, Y. B. He, and B. H. K. Lee, J. Sound Vib. **320**, 163 (2009).
[38] T. Kalmar-Nagy, G. Stepan, and F. Moon, Nonlinear Dynamics **26**, 121 (2001).
[39] F. A. Jafri, A. Shukla, and D. F. Thompson, Nonlinear Dynamics **50**, 627 (2007).
[40] S. Baer, T. Erneux, and J. Rinzel, Siam J. Appl. Math. **49**, 55 (1989).